

# The magnetic and crystal structure of azurite $\text{Cu}_3(\text{CO}_3)_2(\text{OH})_2$ as determined by neutron diffraction

K.C. Rule<sup>1</sup>, M. Reehuis<sup>1</sup>, M.C.R. Gibson<sup>1,2</sup>, B. Ouladdiaf<sup>3</sup>, M.J. Gutmann<sup>4</sup>,  
J.-U. Hoffmann<sup>1</sup>, S. Gerischer<sup>1</sup>, D.A. Tennant<sup>1,2</sup>, S. Süllo<sup>5</sup>, M. Lang<sup>6</sup>

<sup>1</sup>*Helmholtz-Zentrum Berlin, Berlin, Germany*

<sup>2</sup>*Institut für Festkörperphysik,  
TU Berlin, Berlin, Germany*

<sup>3</sup>*Institut Laue-Langevin,  
rue Jules Horowitz, Grenoble, France*

<sup>4</sup>*ISIS, Rutherford Appleton Laboratories, Chilton, UK*

<sup>5</sup>*Institut für Physik der Kondensierten Materie,  
TU Braunschweig, Braunschweig, Germany*

<sup>6</sup>*Goethe Universität, Frankfurt(M), SFB/TR 49, Germany*

Here we present neutron diffraction results on the mineral azurite. We have found that the crystal structure of azurite can be described in the space group  $P2_1$  which is the next lower symmetric group of  $P2_1/c$  as found in earlier work. This small change in symmetry does not greatly influence the lattice parameters or atomic fractional coordinates which are presented here for single crystal diffraction refinements. The ordered magnetic moment structure of this material has been determined and is comprised of two inequivalent magnetic moments on copper sites of magnitude 0.68(1) and 0.25(1)  $\mu_B$ . This result is discussed in terms of the anisotropic exchange and Dzyaloshinskii-Moriya interactions. It is found that the system is likely governed by one-dimensional behaviour despite the long-range ordered ground state. We also highlight the significance of strain in this material which is strongly coupled to the magnetism.

PACS numbers: 75.25.-j 75.50.Ee 61.05.fm 75.30.Et

Low-dimensional, quantum spin systems have garnered much attention of late from both experimentalists and theorists alike. One such material is azurite,  $\text{Cu}_3(\text{CO}_3)_2(\text{OH})_2$ , a natural mineral which has been proposed as an experimental realization of the 1D distorted diamond chain model. Interest in the magnetic properties of this material began in the 1950s when an ordered antiferromagnetic (AFM) ground state was observed below 1.9 K.<sup>1,2</sup> From these studies, a detailed description of the magnetic moment structure was never revealed however it has been speculated that the low ordering temperature may result from frustration in the diamond arrangement of spin-1/2  $\text{Cu}^{2+}$  ions<sup>3</sup>. Early susceptibility measurements indicated that the coupling of spins within the chain could be described with alternating dimers and monomers<sup>4</sup> (Fig. 1). This was later confirmed by magnetization measurements which revealed a distinct plateau at 1/3 the saturation magnetization indicating a polarization of the monomer spins within an applied magnetic field<sup>5</sup>.

More recently, interest in azurite has been renewed with an ongoing debate about the relative strength of the exchange interactions in this material as defined in Fig. 1<sup>5-9</sup>. Current consensus is that this system cannot be described in terms of a simple isotropic exchange chain Hamiltonian, but rather that inter-chain coupling and anisotropic exchange must also be taken into account when describing this material. A detailed understanding of the magnetic structure, as presented here, may provide further useful material in the construction of an effective

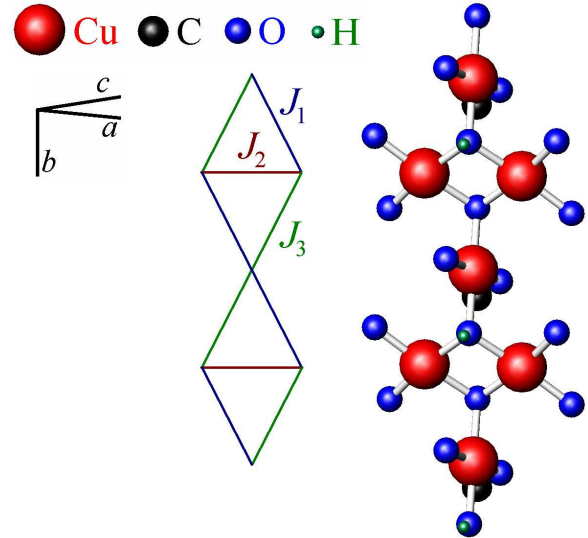


FIG. 1: (Colour online) Diamond chain model showing the relative exchange interactions. It is now widely believed that  $J_2$  is the strongest interaction in azurite.

Hamiltonian to describe this system.

To fully describe the magnetism in azurite, a complete understanding of the structural properties is also necessary. A definitive set of lattice parameters and atomic positions should provide an accurate input for exchange

coupling calculations. Recently evidence of magnetoelastic coupling in this material has been revealed<sup>10</sup>. Confirmed by preliminary neutron scattering investigations, the structural strain in this material coincides with the onset of magnetic ordering<sup>12</sup>. It is therefore possible that the structure of this material is appreciably different below  $T_N$  compared with the structure published for room temperature<sup>13</sup>. Given the interest in predicting the magnetic properties of azurite from structural considerations alone it seems prudent to obtain accurate structural data on azurite in its magnetically ordered state. Here we present the results of a neutron diffraction study of azurite at temperatures above and below  $T_N$ , revealing further evidence of structural distortion in addition to the ordered magnetic ground state.

The sample used in this study was cut from a large high-quality crystal of azurite which has been used in previous studies<sup>7</sup>. The sample was roughly cubic in shape (dimensions  $\sim 3 \times 4 \times 3$  mm) and mounted on a copper pin which offered good thermal conductivity. Diffraction measurements were performed on both the time-of-flight (TOF) instrument SXD at ISIS in the UK and the four-circle diffractometer D10 at Institut Laue-Langevin (ILL) in France. Additional diffraction measurements were also conducted using the E1 triple axis spectrometer (TAS) at Helmholtz Zentrum Berlin (HZB), Germany.

#### A. TOF diffractometer measurements

The Single Crystal Diffractometer SXD combines the time-sorted Laue method with a large array of position sensitive detectors to allow access to large volumes of reciprocal space in one simultaneous measurement. Using this instrument, the sample is illuminated by a white beam of neutrons with a wavelength range 0.2-10.0 Å. A full data set of Bragg peak intensities was measured at both 1.5 and 5 K for a comparison of the structural parameters above and below the Néel temperature.

The crystal structure of azurite was already determined in the late 1950s by Gattow and Zeeman<sup>11</sup>. It was found that azurite crystallises in the monoclinic space group  $P2_1/c$  (No. 14). This space group was confirmed by Zigan *et al.*<sup>13</sup> and Belokoneva *et al.*<sup>14</sup>. However the data from SXD have revealed that Bragg peaks of index-type  $[h0l]$  with  $l$  odd were present in the scattering profile despite being forbidden by the  $P2_1/c$  space group. This observation clearly indicates the loss of the  $c$ -glide plane of  $P2_1/c$ . Group-subgroup relations between the space groups showed that  $\text{Cu}_3(\text{CO}_3)_2(\text{OH})_2$  actually crystallises in the next lower symmetric space group  $P2_1$  (No. 4). These reflections, although of relatively weak intensity, were observed at both 1.5 K and 5 K and indicate azurite retains this symmetry both above and below the Néel temperature. The observation of these peaks with the TOF method is unambiguous – the measured intensity cannot be attributed to higher-order scattering contamination, as it might with other diffraction tech-

niques. In contrast, the ‘forbidden’ reflections have been observed previously in the single crystal neutron diffraction study of Zigan *et al.*<sup>13</sup> but were attributed to higher-order scattering contamination. The lattice parameters for both space groups have been refined from the powder neutron diffraction data<sup>12</sup>, however despite the change in symmetry group the lattice parameters were the same within error. For the  $P2_1$  refinement of the powder neutron diffraction data taken at 1.28 K, the lattice parameters were  $a = 4.99995(11)$  Å  $b = 5.82256(14)$  Å  $c = 10.33723(19)$  Å with  $\beta = 92.2103(17)^\circ$ .

The atomic fractional coordinates were refined from approximately 1800 unique structural reflections at the two measured temperatures of 1.5 and 5 K using the analysis program JANA2006<sup>17</sup>. In the analysis of the structural Bragg peak intensities, information from data sets collected at different orientations of the crystal are not merged resulting in a large data set and complex wavelength-dependent extinction corrections. This, coupled with additional wavelength dependent corrections, typically gives poorer  $R_F$ -factors for TOF methods when compared to monochromatic techniques. The  $R_F$ -factor is a measure of the agreement between the observed and calculated structure factors for a particular crystal structure. Refinements using the  $P2_1/c$  space group gave a reliability of  $R_F \approx 0.080$  and compare favourably with the powder refinement as seen in Table I. The refinement of the SXD data using the  $P2_1$  space group gave unphysical anisotropic thermal parameters and as such did not give accurate positional parameters. The powder data of  $\text{Cu}_3(\text{CO}_3)_2(\text{OH})_2$  were also refined in the space group  $P2_1$ . However due to a poor ratio  $p/n$  less than 9 ( $p$  = number of refined parameters,  $n$  = number of observed structure factors) we were not able to reach accuracies for the positional parameters below  $\sigma = 0.028$ . Therefore, the positional parameters of azurite from both the powder data and the SXD data obtained for the space group  $P2_1$  are not listed in the present work.

Using the TOF technique with SXD, it was also possible to observe and index the magnetic reflections thereby confirming the propagation vector of  $\mathbf{k} = (\frac{1}{2} \frac{1}{2} \frac{1}{2})$ , as has been observed in neutron diffraction measurements previously<sup>12</sup>. For absolute accuracy in the structure factors and somewhat more precise atomic parameters further diffraction measurements at a continuous source were also conducted.

#### B. Four-circle diffractometer measurements

Using D10 at the ILL, with its dilution  $^3\text{He}$  cryostat, it was possible to determine structural and magnetic properties well below the ordering temperature of 1.87 K. This instrument uses a Cu-monochromator selecting the single neutron wavelength  $\lambda = 1.26$  Å selection of half-integer reflections and reflections forbidden by the

TABLE I: Positional and thermal parameters of  $\text{Cu}_3(\text{CO}_3)_2(\text{OH})_2$  as obtained from the structure refinements of single-crystal (on both D10 and SXD) and powder data in the monoclinic space groups  $P2_1/c$ . The isotropic thermal parameters  $U$  are given in units of  $100 \text{ \AA}^2$ . For the refinement several thermal parameters were constrained to be equal. In these cases the standard deviation is listed only for one of the equal parameters.

Atom	site	Powder data at 1.28 K				Single-crystal data at 5 K (SXD)				Single-crystal data at 200 mK (D10)			
		$x$	$y$	$z$	$U$	$x$	$y$	$z$	$U$	$x$	$y$	$z$	$U$
Cu1	2a	0	0	0	0.40(4)	0	0	0	0.14(1)	0	0	0	0.12(3)
Cu2	4e	0.2508(6)	0.4967(5)	0.0834(3)	0.40	0.2515(3)	0.4976(1)	0.08324(9)	0.25(1)	0.2516(2)	0.4977(2)	0.0834(1)	0.12
C	4e	0.3308(6)	0.2994(5)	0.3192(3)	0.63(7)	0.3294(3)	0.2993(2)	0.3180(1)	0.26(2)	0.3303(2)	0.2992(2)	0.3178(1)	0.24(3)
O1	4e	0.0975(7)	0.3972(6)	0.3318(3)	0.60(3)	0.1012(4)	0.3991(2)	0.3310(1)	0.36(2)	0.1016(3)	0.3992(2)	0.3309(2)	0.31(3)
O2	4e	0.0762(7)	0.8126(6)	0.4451(3)	0.60	0.0741(4)	0.8126(2)	0.4450(1)	0.25(2)	0.0743(3)	0.8119(2)	0.4450(2)	0.28(4)
O3	4e	0.4518(6)	0.2098(6)	0.4183(3)	0.60	0.4500(4)	0.2085(2)	0.4176(1)	0.35(2)	0.4503(3)	0.2093(2)	0.4179(2)	0.30(3)
O4	4e	0.4339(6)	0.2949(6)	0.2065(3)	0.60	0.4310(4)	0.2937(1)	0.2068(1)	0.37(2)	0.4317(3)	0.2946(2)	0.2072(2)	0.37(4)
H	4e	0.182(1)	0.800(1)	0.3709(7)	1.75(15)	0.187(1)	0.7996(5)	0.3682(3)	1.72(6)	0.1833(7)	0.7996(6)	0.3686(4)	1.75(7)

$P2_1/c$  space group were also measured to ensure an accurate evaluation of the higher order scattering intensity and structural symmetry respectively. Multiple scattering could be excluded by the use of psi scans. A number of weaker structural peaks at higher scattering angles were also measured as the effects of extinction on such peak intensities are less significant. It was again found that the 'forbidden' reflections had a significant intensity (Fig. 2) that could not be accounted for by the (negligible) higher-order scattering. The magnetic reflections and a further set of structural Bragg peaks were measured at a wavelength of  $2.36 \text{ \AA}$  using a pyrolytic graphite monochromator and filter to suppress higher-order scattering contamination. A full data set of nuclear reflections taken at  $2.36 \text{ \AA}$  were used to determine precisely the overall scale factor which could then be used to analyse the magnetic moment values. Due to the higher flux from the PG-monochromator, a good signal to noise ratio was obtained, and thus we were able to measure the relatively weak magnetic Bragg reflections with good accuracy.

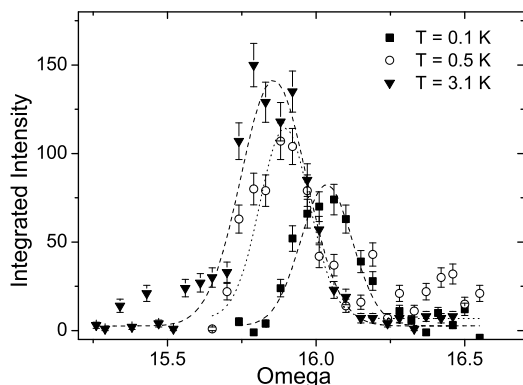


FIG. 2: Intensity profile of the  $[101]$  Bragg reflection at temperatures above and below  $T_N$ . This reflection is forbidden for the  $P2_1/c$  space group but allowed for  $P2_1$ . Lines are guides to the eyes.

### C. Crystal structure and extinction

The crystal structure of  $\text{Cu}_3(\text{CO}_3)_2(\text{OH})_2$  was refined using the data from D10 collected at 200 mK and 5 K. The peak integration was performed using two different methods, the SEED program<sup>15</sup> and the RACER program<sup>16</sup>, in order to optimise the quality of data for structural refinements. However both methods of peak integration gave very similar fits to the structural refinement. Refinements were carried out initially in the monoclinic space group  $P2_1/c$  as done earlier by Zigan *et al.*<sup>13</sup> and Belokoneva *et al.*<sup>14</sup>. The lattice parameters were taken from the powder data as presented above since it was clear that extinction effects significantly affected the single-crystal data resulting in a poor refinement. Since secondary extinction is not present in polycrystalline samples the powder refined parameters were considered to be more accurate.

The significance of extinction effects in this material was revealed on measuring the temperature dependence of the Bragg peak intensities. As discussed in previous work<sup>12</sup>, such a large intensity increase below  $T_N$  cannot be due to magnetic ordering alone. However since the intensity change coincides with the magnetic ordering transition it is clear that the structure and magnetism of azurite are closely coupled. In Fig. 3, for example, we see a 30% increase in the intensity of the  $[120]$  peak on cooling the single crystal sample below  $T_N$  and an 80% increase in the intensity of the  $[040]$ . In fact only structural Bragg reflections with a component along  $[0k0]$  were effected by the extinction effects. Due to the close coupling between the extinction and the onset of magnetic order, it is likely that the magnetoelastic coupling is mediated by the diamond chain units which propagate along the crystallographic  $b$ -axis parallel to  $[0k0]$ . Surprisingly, additional yet weak intensity changes were also observed below 0.5 K on the  $[h00]$  peaks suggesting that there may also be strain coupled to the  $a$ -direction. This appears at the same temperature as an anomaly observed in recent ultrasonic measurements<sup>19</sup> however the nature of this anomaly is not yet known and requires further

investigations. For the extinction correction in the structural refinement the formalism of Zachariasen (type I) was used<sup>18</sup>. The refineable parameter  $g$  in this formalism is related to the mosaic distribution and assumes a Gaussian distribution of mosaic blocks within the sample. An absorption coefficient  $\mu = 0.158 \text{ mm}^{-1}$ , was also used for refinements.

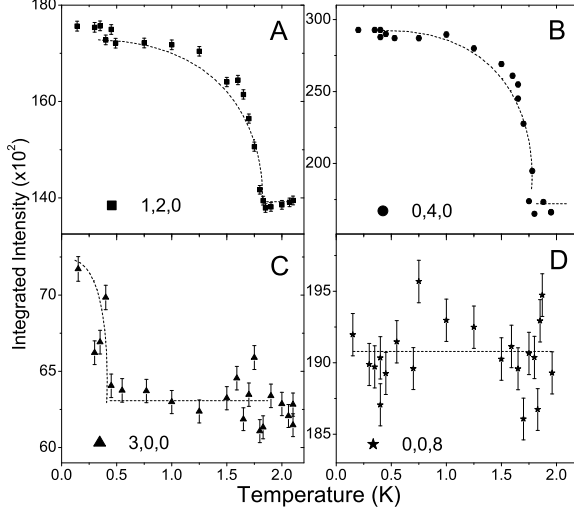


FIG. 3: The temperature dependence of the integrated intensity of the (120), (040), (008) and (300) Bragg peaks of  $\text{Cu}_3(\text{CO}_3)_2(\text{OH})_2$ , as obtained from single-crystal neutron diffraction experiments. Note that the large increase in intensity at the Néel temperature is only observed for peaks with a non-zero  $k$ -index, while peaks with a non-zero  $h$ -index also exhibit a change in intensity below 0.5K. Lines are a guide to the eye.

For the refinement of the crystal structure at 200 mK a total number of 1771 (845 unique) reflections were used. The refinement of the overall scale factor, extinction parameter and the positional and isotropic thermal parameters resulted in a poor residual  $R_F = 0.089$  ( $R_w = 0.110$ ). The refined extinction parameter ( $g$ ) of about  $1200 \text{ rad}^{-1}$  indicates that extinction is quite strong in azurite. It could be seen that strong reflections of the series ( $h0l$ ) were observed to be systematically weaker than the calculated values while the intensities of the ( $0k0$ ) reflections were calculated to be much stronger than their observations. This clearly highlights the anisotropy of the extinction.

In order to improve the refinements we rejected 123 (58 unique) of the very strong reflections. In Table I it can be seen that the positional and thermal parameters of the different atoms could be determined with good accuracy. The refinement finally resulted in a better residual  $R_F = 0.070$  ( $R_w = 0.069$ ) although the positional parameters obtained from both refinements showed a good agreement. Further, the positional parameters of

the single-crystal data also show a good agreement with the values obtained from the neutron powder diffraction data collected at 1.28 K and the single-crystal data from SXD (Table I). But despite the fact that the refinement quality from the single-crystal data was reduced due to anisotropic extinction we were able to determine the positional parameters with much better accuracy than from the powder diffraction study (Table I). The refinements of the D10 single-crystal data collected at 5 K resulted in a strongly enlarged extinction parameter of about  $4000 \text{ rad}^{-1}$  which is clearly also affecting the fit parameters of the SXD data.

The refinement of the single crystal data using the  $P2_1$  space group involved a relatively large number of 62 positional and isotropic parameters. Since the obtained parameters were highly correlated, with correlation coefficients exceeding 90 %, we used constraints to restrict the values of particular thermal parameters (Table II). Finally a refinement of a total of 54 parameters resulted in a residual  $R_F = 0.067$  ( $R_w = 0.063$ ). The results of the refinement of the D10 data for the  $P2_1$  symmetry group are summarised in Table II.

The positional parameters of the copper atoms for the two different space groups  $P2_1/c$  and  $P2_1$  are given in Tables I and II. In  $P2_1/c$  the Cu1-atoms are located at the special Wyckoff position  $2a(0, 0, 0)$ . Therefore in this space group the interatomic distances to the next neighboring Cu1'-atoms in  $(0, \frac{1}{2}, \frac{1}{2})$ ,  $(0, -\frac{1}{2}, \frac{1}{2})$ ,  $(0, \frac{1}{2}, -\frac{1}{2})$ , and  $(0, -\frac{1}{2}, -\frac{1}{2})$  are identical [ $d_{\text{Cu1-Cu1}'} = 5.9321(1) \text{ \AA}$ ]. In the space group  $P2_1$  the Cu1-atoms are located at the general Wyckoff position  $2a(x, y, z)$ . In Table II it can be seen that the  $x$ -parameter does not show any change from the ideal position  $x = 0$ . On the other hand the  $y$ - and  $z$ -values show a slight shift from the ideal position  $y = 0$  and  $z = \frac{1}{4}$  (in  $P2_1$ ) or  $z = 0$  (in  $P2_1/c$ ) of about  $3 - 4\sigma$ . In the lower symmetric space group  $P2_1$  one finds two different interatomic distances. The distances between Cu1 in  $(0, 0, 0)$  and the Cu1'-atoms in  $(0, \frac{1}{2}, \frac{1}{2})$ , and  $(0, -\frac{1}{2}, \frac{1}{2})$  are the same [ $d_1 = 5.913(4) \text{ \AA}$ ]. But along the opposite  $z$ -direction the distance to the Cu1'-atoms in  $(0, \frac{1}{2}, -\frac{1}{2})$ , and  $(0, -\frac{1}{2}, -\frac{1}{2})$  is  $d_2 = 5.952(4) \text{ \AA}$  where  $d_1$  and  $d_2$  are plotted in the  $bc$ -plane in figure 6. In fact our study shows that the shift from the ideal position is relatively weak. However it is interesting to note that the lower symmetric setting allows a dimerization of monomer Cu1-sites. On the other hand the Cu2-atoms (in  $P2_1/c$ ) are located in the general Wyckoff position  $4c(x, y, z)$ , while in the lower symmetric space group  $P2_1$  this position splits into two different positions Cu21 and Cu22, but both at the general position  $2a(x, y, z)$ . In Tables I and II it can be seen that the Cu2-atoms in the two representations show a good agreement, with respect to their standard deviations. Please note that one finds the relation  $z'(\text{Cu2}) = z(\text{Cu21 or Cu22}) - \frac{1}{4}$  for the two different representations.

TABLE II: Positional and thermal parameters of  $\text{Cu}_3(\text{CO}_3)_2(\text{OH})_2$  as obtained from the structure refinements of single-crystal data taken at 200 mK using the monoclinic space group  $P2_1$ . For the refinement several thermal parameters,  $U$  (given in  $100 \text{ \AA}^2$ ), were constrained to be equal. In these cases the standard deviation is listed only for one of the equal parameters.

Atom	site	$x$	$y$	$z$	$U$
Cu1	2a	0.0000(5)	0.0015(6)	0.2511(3)	0.13(4)
Cu21	2a	0.2514(4)	0.4985(5)	0.3336(2)	0.16(3)
Cu22	2a	0.7488(4)	0.5027(5)	0.1668(3)	0.16
C11	2a	0.3306(5)	0.3012(5)	0.5685(3)	0.21(3)
C12	2a	0.6691(5)	0.7026(5)	0.9334(3)	0.21
O11	2a	0.0997(5)	0.3921(5)	0.5815(4)	0.27(3)
O12	2a	0.8954(5)	0.5949(5)	0.9198(4)	0.27
O21	2a	0.0762(5)	0.8100(5)	0.6957(4)	0.33(4)
O22	2a	0.9269(6)	0.1853(5)	0.8065(4)	0.33
O31	2a	0.4518(5)	0.2068(6)	0.6700(4)	0.33(3)
O32	2a	0.5518(5)	0.7891(6)	0.8341(4)	0.33
O41	2a	0.4366(5)	0.2915(5)	0.4564(4)	0.34(3)
O42	2a	0.5732(5)	0.2915(5)	0.4564(4)	0.34
H11	2a	0.1768(12)	0.8088(11)	0.6129(7)	1.60(7)
H12	2a	0.8117(12)	0.2113(23)	0.8754(7)	1.60(7)

#### D. High magnetic field measurements

Further insight into the magnetic and structural interdependence can be taken from the field dependence of the intensity of the [120] structural Bragg peak. To investigate the effects of applied magnetic fields on the structure of azurite, single-crystal neutron diffraction was carried out using the E1 triple axis spectrometer at HZB (neutron wavelength  $\lambda = 2.428 \text{ \AA}$ ). The small azurite single crystal remained on the copper mount with a horizontal  $a^* - b^*$  scattering plane, such that magnetic fields up to 14 T were applied perpendicular to  $b^*$ , *i.e.*, perpendicular to the chain direction. In this geometry the  $1/3$  magnetization plateau, where the monomer spins are polarised with the applied field, ranges from 11 to 30 Tesla<sup>5</sup>. A temperature dependence of these applied field effects was also conducted for temperatures up to 5 K. With the aid of a  $^3\text{He}$  cryostat insert, base temperatures of  $T \sim 0.5 \text{ K}$  were attained.

The left panel of figure 4 displays the integrated intensity of the [120] nuclear Bragg reflection as a function of field while the right panel shows the temperature dependence. The intensity has been normalised either to the peak intensity at 14 T or at 2 K, since no further intensity changes were observed well within the plateau phase and above the ordering temperature respectively. At temperatures approaching  $T_N$ , the field at which the intensity becomes invariant is reduced. Both data sets have been combined in Fig. 5 for the full field and temperature range.

While the atomic fractional coordinates do not change significantly within the accuracy of these neutron scattering experiments, changes in the lattice parameters have been observed<sup>10,12</sup>. These slight changes may facilitate

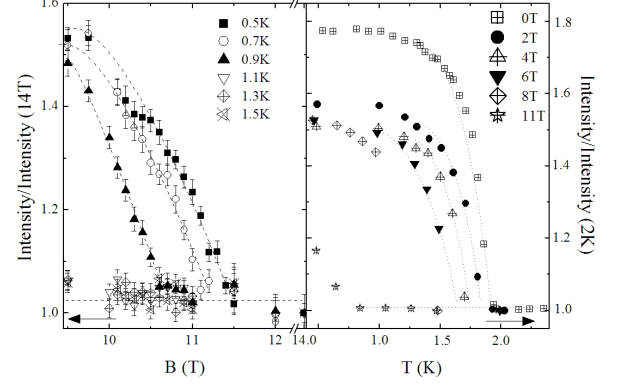


FIG. 4: (left) The field (left) and temperature (right) dependence of the normalized integrated intensity of the [120] Bragg peak of  $\text{Cu}_3(\text{CO}_3)_2(\text{OH})_2$  near the plateau field range from single crystal neutron diffraction. Lines are guides to the eye.

the formation of the mosaic blocks within the crystal which in turn become misaligned on a macroscopic scale increasing the mosaicity of the sample. Thus as azurite enters the AFM ground state in zero field, we see a large intensity increase as the extinction effects are reduced due to shifts in the lattice parameters.

As a magnetic field is applied perpendicular to the  $b$ -axis, the AFM correlations between monomer spins gives way to ferromagnetic correlations which in turn allows the lattice to return to a state with fewer mosaic block discontinuities and therefore increased extinction effects. At temperatures closer to  $T_N$ , the magnetic interactions are weaker and thus a lower applied field is required to reduce the spread of mosaic blocks. This may explain why we see a reduction in intensity of the nuclear [120] Bragg peak in applied fields as seen in figure 5. Thus the change in intensity with applied field, whilst being an extinction effect, highlights the phase boundary of the AFM state in azurite. It is also worthwhile to note that the intensity of the [120] Bragg peak in the plateau phase is the same as in the paramagnetic, low field phase indicating that the mosaicity in both phases is the same.

#### E. Magnetic structure

The magnetic diffraction results from D10 were also treated with the RACER program to yield integrated intensities which were then refined using FULLPROF. The scale factor was obtained by refining the nuclear structure with  $2.36 \text{ \AA}$  neutrons, while keeping all other parameters constant from the fit taken with  $1.26 \text{ \AA}$  neutrons. The propagation vector  $k = (\frac{1}{2} \frac{1}{2} \frac{1}{2})$ , obtained from previous diffraction measurements on both E2 at HZB<sup>12</sup> and SXD at ISIS, was used to refine the magnetic moment structure. The refined magnetic structure, with a Bragg  $R$ -factor of 6.9%, is shown in figure 6. The Bragg  $R$ -factor compares the measured and calculated magnetic intensi-

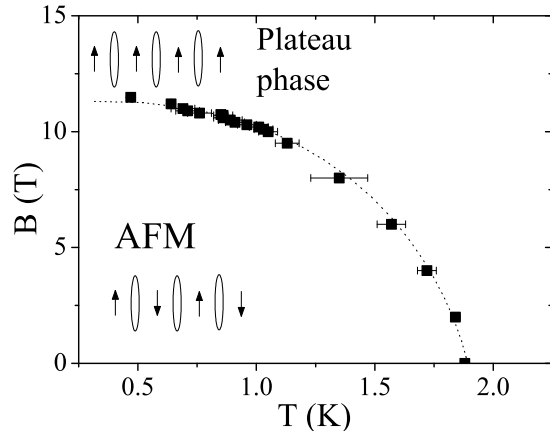


FIG. 5: An indirect measure of the phase diagram as inferred from the field and temperature dependence of the integrated intensity of the [120] peak. Line is a guide to the eye. Ovals and arrows represent the Cu-dimer pairs and the relative orientation of the Cu-monomers respectively.

ties rather than the structure factors as defined by the  $R_F$ -factor. In figure 6 the blue (dark) spins represent the Cu(1) sites which we commonly refer to as the monomer sites and the red (light) spins represent the Cu(2) sites which form dimerised pairs. Along the chain direction, the monomer spins are collinear and oriented in the  $a$ -plane with a slight canting along the  $b$ -direction. The monomer spins lie with an easy axis at an angle of  $55 \pm 3^\circ$  from the  $c$ -axes which corresponds within error to the value of  $52^\circ$  found from magnetisation measurements<sup>4</sup>.

The magnetic moment on the monomer sites, is  $0.68 \mu_B$ , while the moment on the dimer sites is  $0.25 \mu_B$ . A moment size of  $0.68 \mu_B$  is consistent with magnetic moments found in other cuprate systems where the reduction from the  $1 \mu_B$  expected for a  $\text{Cu}^{2+}$  ion can be attributed to zero point spin fluctuations and/or covalency effects<sup>20,21</sup>. Note that the size of moment on the dimers determined in this study, while significantly reduced from the monomer value, is somewhat larger than the moment found for azurite in its plateau phase from NMR<sup>22</sup>. This reduction may be caused by mean field effects. In the plateau phase, the monomers form a ferromagnetic chain which may influence the overall moment at the dimer sites. In low fields, when the monomers are coupled antiferromagnetically, the mean field effects are somewhat different.

All magnetic Bragg peaks showed an increase in intensity below the ordering temperature as expected for a second order phase transition. Since the influence of extinction is roughly proportional to the intensity of the Bragg peaks, the effect of the anisotropic extinction on the overall magnetic refinement result is minimal.

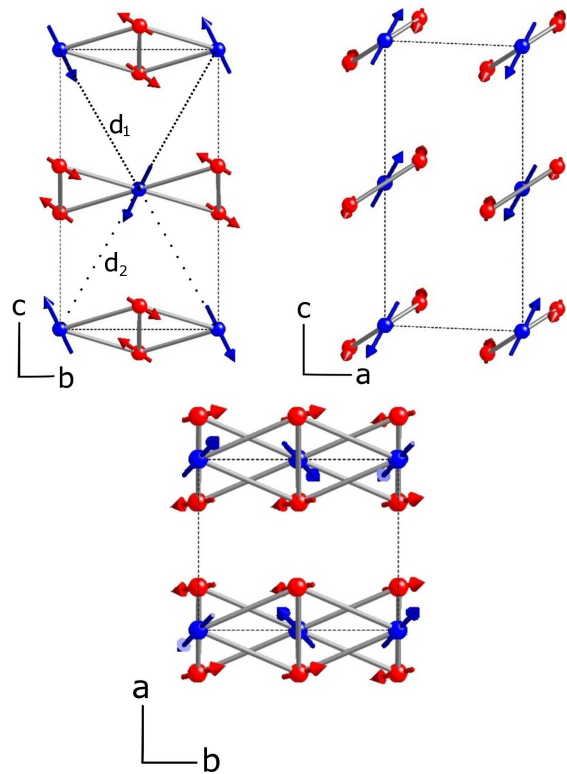


FIG. 6: (Colour online) The magnetic structure of azurite, shown in the  $b$ - $c$ ,  $a$ - $c$  and  $a$ - $b$  planes (l-r.). The monomer sites, with a moment size of  $0.68 \mu_B$ , are represented by the blue (dark) spheres, while the dimer sites ( $0.25 \mu_B$ ) are represented by the red (light). The monomer spins on alternate  $a - b$  planes are aligned perpendicularly. The lengths  $d_1$  and  $d_2$  have been determined for the  $P2_1$  space group in section C.

TABLE III: Table of the magnetic spin components of the monomer (Cu(1)) and dimer (Cu(2)) spins at the atomic fractional coordinate positions of Cu(1) (0, 0, 0) and Cu(2) (0.251, 0.498, 0.083).

Site	Spin-component ( $\mu_B$ )
Cu(1) <sub>x</sub>	0.438 (3)
Cu(1) <sub>y</sub>	0.360 (3)
Cu(1) <sub>z</sub>	0.393 (3)
Cu(2) <sub>x</sub>	0.232 (2)
Cu(2) <sub>y</sub>	0.044 (2)
Cu(2) <sub>z</sub>	0.093 (2)

## F. Discussion

For a reduced moment size of  $0.25 \mu_B$  we can consider that the Cu(2) sites (represented by the red spins in figure 6) are coupled primarily into spin singlet states with their nearest neighbouring Cu(2) spin in the diamond unit. The observation of a finite spin polarisation implies that the singlet state is subject to some perturbative effect which induces the non-negligible spin moment.



Assuming the interchain coupling is negligible in comparison with the intrachain coupling, the staggered field of the neighbouring monomer spin sites may be responsible for this perturbation.

Considering at first only Heisenberg exchange couplings, the expectation values of the spin moment on the dimer atoms in the staggered field of the neighbouring monomer sites can be calculated from the Hamiltonian

$$H = J_2 \vec{S}_1 \cdot \vec{S}_2 + (J_1 - J_3) \langle S_m^z \rangle S_1^z - (J_1 - J_3) \langle S_m^z \rangle S_2^z \quad (1)$$

where the ordered moment on the monomer sites defines the  $z$ -axis and is of magnitude  $\langle S \rangle$ . For all nonzero  $\langle S \rangle$  a staggered moment on sites  $S_1$  and  $S_2$  is established for the ground state collinear with the monomer spins. Whilst the ratio of  $(J_1 - J_3)/J_2 = 1/2.8$  implied by the relative ordered moments on dimer and monomer spins is in rather good agreement with the exchange couplings determined by Rule *et al.*<sup>7</sup> the non-collinearity requires the introduction of other exchange terms.

A likely scenario involves Dzyaloshinskii-Moriya (DM) interactions which strongly influence the non centrosymmetric  $J_1$  and  $J_3$  exchange interactions as outlined in Figure 7. Taking the extra exchange terms of the type  $\vec{D}_1 \cdot (\vec{S}_{m1} \times \vec{S}_1 + \vec{S}_{m2} \times \vec{S}_2) + \vec{D}_3 \cdot (\vec{S}_{m2} \times \vec{S}_1 + \vec{S}_{m1} \times \vec{S}_2)$  and using the fact that  $\vec{S}_{m1} = -\vec{S}_{m2} = (0, 0, \langle S_m \rangle)$  then the Hamiltonian becomes

$$\begin{aligned} H = J_2 \vec{S}_1 \cdot \vec{S}_2 &+ (D_1^y - D_3^y) \langle S_m^z \rangle (S_1^x - S_2^x) \\ &- (D_1^x - D_3^x) \langle S_m^z \rangle (S_1^y - S_2^y) \\ &+ (J_1 - J_3) \langle S_m^z \rangle (S_1^z - S_2^z) \end{aligned}$$

This then causes a tilting of the dimer spins compared to the monomer  $z$  direction along the new effective staggered field  $(D_1^y - D_3^y, D_1^x - D_3^x, J_1 - J_3) \langle S_m^z \rangle$  direction. The significant tilting observed would imply that the DM interactions are of order  $(J_1 - J_3)$ , *i.e.* a few K.

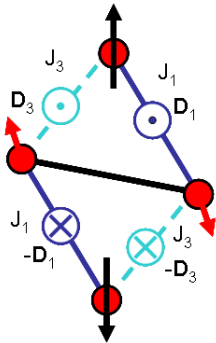


FIG. 7: (Colour online) Dzyaloshinskii-Moriya (DM) interactions on the diamond shape units where the vertical direction corresponds to the  $b$ -axis. We define the notation of  $\odot$  and  $\otimes$  to represent antiparallel vectors since the actual orientation of the DM vector is not known.

A further consequence of including DM interactions is that the effective Hamiltonian of the monomer spins

loses full rotational symmetry and results in an XXZ type Hamiltonian with planar character (the easy plane being perpendicular to  $(D_1 - D_3)$ ). To explain the spin flop type behaviour observed in azurite<sup>25</sup> other terms resulting in an easy axis are needed, either from the symmetry lowering to  $P2_1$ , interchain coupling, or further anisotropies. The application of non-commuting magnetic fields to such low dimensional XYZ antiferromagnets, where  $J_x \neq J_y \neq J_z$ , have been observed to cause remarkable behaviour in the vicinity of quantum critical points<sup>26,27</sup> and azurite may well provide an important new system in this line. Here, for example, the quantum phase transition into the plateau phase could take on a transverse Ising character<sup>26</sup>. We defer further discussion of the full derivation of the Hamiltonian to a future paper on the dynamics in azurite.

The question remains as to what extent the diamond chains in azurite can be considered to be modeled reasonably as a one-dimensional system. The Mermin-Wagner theorem indicates that truly one-dimensional systems cannot enter a long ranged ordered state due to quantum fluctuations<sup>24</sup>, however experimentally, materials such as azurite which display quasi-1D characteristics clearly enter a 3D Néel state. The significance of quantum fluctuations in a given system may be established from the ratio of the Curie-Weiss temperature to the Néel temperature. It has been found from susceptibility measurements that for azurite this value is roughly  $-\Theta_{CW}/T_N \approx 5$ , implying that quantum fluctuations should play a significant role for all temperatures below  $\Theta_{CW}$ <sup>28</sup>.

Further, the relative strengths of inter- and intra-chain couplings may be inferred from the ordered magnetic moment for comparatively weakly coupled chains<sup>29,30</sup>. The effective one-dimensional chain model provides a reasonable description of the system with coupling  $J_{mono} = 0.87$  meV, determined previously from inelastic neutron scattering<sup>7</sup>. Taking the measured moment of  $m_0 = 0.68$  bohr magnetons, then an effective tetragonal interchain coupling of  $|J_\perp| = 0.097$  meV would be required to account for the ordering strength. It should be noted that Ising anisotropies would serve to increase the ordered moment for the same interchain coupling.

## G. Summary

In summary, we have observed that azurite belongs to a lower symmetry space group  $P2_1$ . We have revealed the significance of magnetoelastic strain in this material as observed by field and temperature dependent extinction effects. Also presented here is the ground state magnetic structure of azurite which confirms that the diamond chain arrangement of magnetic  $\text{Cu}^{2+}$  sites in this material can, to some extent, be considered as an alternating arrangement of dimer and monomer entities. The ordered magnetic structure may also indicate the presence of competing interactions between the chains in this material and the significance of anisotropic exchange.

Comparison of the magnitude of the ordered magnetic moment with existing theories of coupled quantum spin chains implies that the interchain coupling is weak in this material and that the system may thus be considered one-dimensional. The magnitude and orientation of the magnetic moments in azurite points to additional anisotropy terms in the Hamiltonian. Additional diffraction studies will be required to determine the ordered magnetic state of this intriguing material in its plateau phase.

## Acknowledgments

We would like to thank Wolfgang Jauch for valuable discussions. The authors are grateful for the local support staff at ISIS, HZB and the ILL. This research was supported in part by the Deutsche Forschungsgemeinschaft DFG under Grant No. SU229/9-1.

- 
- <sup>1</sup> R. D. Spence, and R.D. Ewing, Phys. Rev. **112**, 1544 (1958).
  - <sup>2</sup> H. Forstat, G. Taylor and B. R. King, J. Chem. Phys. **31**, 929 (1959).
  - <sup>3</sup> H. Kikuchi, Y. Fujii, M. Chiba, S. Mitsudo and T. Idehara, Physica B **329**, 967 (2003).
  - <sup>4</sup> E. Frikkee and J. Handel, Physica, **28**, 269 (1962).
  - <sup>5</sup> H. Kikuchi, Y. Fujii, M. Chiba, S. Mitsudo, T. Idehara, T. Tonegawa, K. Okamoto, T. Sakai, T. Kuwai, and H. Ohta, Phys. Rev. Lett. **94**, 227201 (2005).
  - <sup>6</sup> B. Gu, and G. Su, Phys. Rev. Lett. **97**, 089701 (2006).
  - <sup>7</sup> K. C. Rule, A. U. B. Wolter, S. Süllow, D. A. Tennant, A. Brühl, S. Köhler, B. Wolf, M. Lang, and J. Schreuer, Phys. Rev. Lett. **100**, 117202 (2008).
  - <sup>8</sup> J. Kang, C. Lee, R.K. Kremer and M-H Whangbo, J. Phys.: Condens. Matter **21**, 392201 (2009).
  - <sup>9</sup> A. Honecker, and A. Läuchli, Phys. Rev. B **63**, 174407 (2001).
  - <sup>10</sup> F. Wolff-Fabris, S. Francoual, V. Zapf, M. Jaime, B. Scott, S. Tozer, S. Hannahs, T. Murphy and A. Lacerda, J. Phys.: Conference Series **150** 042030 (2009).
  - <sup>11</sup> G. Gattow, and J. Zemann, Acta Cryst. **11**, 866 (1958).
  - <sup>12</sup> M. Gibson, K. C. Rule, A. U. B. Wolter, J.-U. Hoffmann, O. Prokhnenko, D. A. Tennant, S. Gerischer, M. Kraken, F. J. Litterst, S. Süllow, J. Schreuer, H. Luetkens, A. Brühl, B. Wolf, and M. Lang, Phys. Rev. B *Rapid Comm.* **81**, (2010).
  - <sup>13</sup> F. Zigan, and H.D. Schuster, Z. Kristallogr. **135**, 416 (1972).
  - <sup>14</sup> E.L. Belokoneva, Y. K. Gubina and J. B. Forsyth, Phys. Chem. Minerals **28**, 498 (2001).
  - <sup>15</sup> J. Peters, Journal of Applied Crystallography, **36**, 1475 (2003).
  - <sup>16</sup> C. Wilkinson, H. Khamis, R.F.D. Stansfield and G.J. McIntyre. J. Appl. Crystallogr. **21**, 471 (1988).
  - <sup>17</sup> V. Petricek, M. Dusek, and L. Palatinus, Jana2006. The crystallographic computing system. Institute of Physics, Praha, Czech Republic (2006).
  - <sup>18</sup> W. H. Zachariasen, Acta Crystallographica, **23**, 4, (1967).
  - <sup>19</sup> P. T. Cong, B. Wolf, U. Tutsch, K. Remović-Langer, J. Schreuer, S. Süllow, and M. Lang J. Phys.: Conf. Ser. **200** 012226 (2009).
  - <sup>20</sup> B. X. Yang, J. M. Tranquada and G. Shirane, Phys. Rev. B **38**, 174 (1988).
  - <sup>21</sup> J. M. Tranquada, A. H. Moudden, A. I. Goldman, P. Zolliker, D. E. Cox, G. Shirane, S. K. Sinha, D. Vaknin, D. C. Johnston, M. S. Alvarez, A. J. Jacobson, J. T. Lewandowski and J. M. Newsam. Phys. Rev. B **38**, 2477 (1988).
  - <sup>22</sup> F. Aimò, S. Krämer, M. Klanjšek, M. Horvatić, C. Berthier, and H. Kikuchi, Phys. Rev. Lett. **102**, 127205 (2009).
  - <sup>23</sup> A. A. Zvyagin and S. -L. Drechsler, Phys. Rev. B **78**, 014429 (2008).
  - <sup>24</sup> N.D. Mermin, H. Wagner, Phys. Rev. Lett. **17**, 11331136 (1966).
  - <sup>25</sup> N.D. Love, T. K. Duncan, P. T. Bailey and H. Forstat, Phys. Lett. **33A**, 290 (1970).
  - <sup>26</sup> M. Kenzelmann, R. Coldea, D. A. Tennant, D. Visser, M. Hofmann, P. Smeibidl, and Z. Tylczynski, Phys. Rev. B **65**, 144432 (2002).
  - <sup>27</sup> R. Coldea, D. A. Tennant, E. M. Wheeler, E. Wawrzynska, D. Prabhakaran, M. Telling, K. Habicht, P. Smeibidl and K. Kiefer, Science **327** 177 (2010).
  - <sup>28</sup> A. P. Ramirez, Annu. Rev. Mater. Sci. **24**, 453 (1994).
  - <sup>29</sup> H. J. Schulz, Phys. Rev. Lett. **77**, 2790 (1996).
  - <sup>30</sup> B. Lake, D. A. Tennant, C. D. Frost and S. E. Nagler, Nature Materials **4**, 329 (2005).
  - <sup>31</sup> D. Coffey, T.M. Rice, F.C. Zhang, Phys. Rev. B **44**, 10112 (1991).



This figure "azuritfig1.jpg" is available in "jpg" format from:

<http://arxiv.org/ps/1010.5340v1>

This figure "DMinteract2.jpg" is available in "jpg" format from:

<http://arxiv.org/ps/1010.5340v1>

This figure "FourPlot2.jpg" is available in "jpg" format from:

<http://arxiv.org/ps/1010.5340v1>

This figure "Forbidden3.jpg" is available in "jpg" format from:

<http://arxiv.org/ps/1010.5340v1>

This figure "phase4.jpg" is available in "jpg" format from:

<http://arxiv.org/ps/1010.5340v1>

This figure "magstruc5.jpg" is available in "jpg" format from:

<http://arxiv.org/ps/1010.5340v1>



This figure "BTDep120b.jpg" is available in "jpg" format from:

<http://arxiv.org/ps/1010.5340v1>